Talanta 122 (2014) 70–79

Contents lists available at ScienceDirect

Talanta

journal homepage: www.elsevier.com/locate/talanta

From multispectral imaging of autofluorescence to chemical and sensory images of lipid oxidation in cod caviar paste

Diego Airado-Rodríguez [a,b,*], Martin Høy [a], Josefine Skaret [a], Jens Petter Wold [a]

[a] Nofima AS, Osloveien 1, N-1430 Ås, Norway
[b] Department of Analytical Chemistry, Faculty of Sciences, University of Extremadura. Avenida de Elvas s/n, E-06006 Badajoz, Spain

ARTICLE INFO

Article history:
Received 9 July 2013
Received in revised form
22 December 2013
Accepted 24 December 2013
Available online 13 January 2014

Keywords:
Multispectral imaging
Autofluorescence
Sensory analysis
Multivariate curve resolution
PLSR

ABSTRACT

The potential of multispectral imaging of autofluorescence to map sensory flavour properties and fluorophore concentrations in cod caviar paste has been investigated. Cod caviar paste was used as a case product and it was stored over time, under different headspace gas composition and light exposure conditions, to obtain a relevant span in lipid oxidation and sensory properties. Samples were divided in two sets, calibration and test sets, with 16 and 7 samples, respectively. A third set of samples was prepared with induced gradients in lipid oxidation and sensory properties by light exposure of certain parts of the sample surface. Front-face fluorescence emission images were obtained for excitation wavelength 382 nm at 11 different channels ranging from 400 to 700 nm. The analysis of the obtained sets of images was divided in two parts: First, in an effort to compress and extract relevant information, multivariate curve resolution was applied on the calibration set and three spectral components and their relative concentrations in each sample were obtained. The obtained profiles were employed to estimate the concentrations of each component in the images of the heterogeneous samples, giving chemical images of the distribution of fluorescent oxidation products, protoporphyrin IX and photoprotoporphyrin. Second, regression models for sensory attributes related to lipid oxidation were constructed based on the spectra of homogeneous samples from the calibration set. These models were successfully validated with the test set. The models were then applied for pixel-wise estimation of sensory flavours in the heterogeneous images, giving rise to sensory images. As far as we know this is the first time that sensory images of odour and flavour are obtained based on multispectral imaging.

1. Introduction

Oxidation of foods is a major cause for limited shelf life. Studies of how oxidation and oxidation processes are affected by packaging, storage conditions and storage time are therefore important to optimise these conditions. Valuable studies depend on relevant and reliable measurement techniques for the quantification of lipid and protein oxidation. A set of methods are established for such, based on chromatography and wet chemistry, however, most of them are destructive, time consuming and not necessarily optimised for complex foods. Sensory analysis is a highly relevant method and in many cases more sensitive than instrumental methods. A drawback is the high cost of a well-trained sensory panel, as well as a rather low capacity with respect to the number of samples that can be analysed per day. A third limitation is the resolution in sample size, there is a limit for how small samples a panel can analyse, which makes it difficult to study for instance the spatial development of an oxidation process. Gradients of photo-oxidation in cheese have been recorded by a sensory panel [1], but this is costly and impractical.

Thus, analytical methodologies able to detect early stages of protein and lipid oxidation in complex food matrices are highly needed, with particular interest in those, which are rapid and non-destructive. In this regard, front-face fluorescence spectroscopy is a potentially attractive technique. Fluorescence spectroscopy is an instrumental technique which has been extensively exploited for studies of molecular structure and function in the discipline of chemistry and biochemistry [2]. Fluorescence measurement can be performed by using either classical right-angle solution fluorescence or front face fluorescence spectroscopy. In classical fluorescence, for sample absorbance lower than 0.05, measurements are performed on solutions, where the intensity of the emitted light is proportional to the florophore concentration [3]. When the absorbance of the sample exceeds 0.05, fluorescence is quenched and spectra are distorted. It is standard practice to dilute the original sample until obtaining an absorbance less than 0.05, nevertheless, results obtained on diluted samples are not always comparable to those obtained with an original sample. To overcome this problem

* Corresponding author.
E-mail addresses: airado@unex.es, dairador@gmail.com (D. Airado-Rodríguez).

0039-9140/$ - see front matter © 2014 Elsevier B.V. All rights reserved.
http://dx.doi.org/10.1016/j.talanta.2013.12.052

and examine intact samples directly, the front-face technique is more appropriate. The technique was originally developed in 1968 [4]. Front-face fluorescence allows measurement of the fluorescence of powdered, turbid, and concentrated samples, as well as complex food matrices such as meat, fish and dairy products [5]. In front-face fluorescence spectroscopy, the surface of a sample is simply illuminated by excitation light, and the emitted fluorescence from the same surface is measured, which minimises reflected light, scattered radiation and depolarisation phenomena.

It has been shown that front-face fluorescence can be used as a method for rapid and non-destructive screening of oxidation in a range of products, such as poultry [6], salmon patè [7], and cheese [8]. Some tertiary oxidation products are fluorescent and enable detection of oxidation in some products with the same sensitivity as e.g. gas chromatography and sensory analysis [7]. In the case of photooxidation, front face fluorescence has the interesting ability to measure simultaneously the photobleaching of active photosensitizers and the formed oxidation products. This has been shown for e.g. butter [9], cheese [10] and cod caviar paste [11]. The use of chemometrics is usually required for interpretation and quantitative modelling of the spectra collected from such untreated systems.

Spectral imaging is an interdisciplinary field comprising image analysis, spectroscopy and chemistry. Spectral imaging is divided into two main techniques: hyperspectral imaging and multispectral imaging. The hyperspectral technique acquires images at numerous (hundreds) continuous wavebands, while the multispectral technique acquires images only at few (normally around 10 or less) discrete wavebands. Or in other words, the hyperspectral technique consists of more finely divided spectral channels than the multispectral one. Thus, a quite high-resolution spectrum can be extracted at each pixel from hyperspectral images, while multispectral images produce a set of isolated data points at each pixel. Hyperspectral data offers more detailed information about a sample object, since it collects images with high spatial and spectral resolution. Nevertheless, it is not very practical to implement the hyperspectral technique for rapid methods development or on-line systems because of the long time required for image acquisition and the big volume of generated data. It is common practice to run hyperspectral imaging studies as a precursor for establishing consistent multispectral imaging methods using a few optimum wavebands for real-time applications.

Multispectral imaging is well known from remote sensing of earth by satellite imagery [12], medical diagnosis [13] and material science [14]. The methodology is typically used for detection of certain features, e.g. such as contamination [15], detailed characterisation of e.g tissue [16,17] or for effective sampling of heterogeneous samples [18]. One challenge with imaging techniques, both multispectral and hyperspectral, compared to regular spectroscopy, is how to calibrate a system to produce quantitative results at pixel level. Multivariate curve resolution (MCR) can be directly applied on images with the aim of decomposing the mixed spectra into pure spectral components as well as the corresponding relative concentrations of each component. This technique has been demonstrated to work well even for hyperspectral images based on front face fluorescence spectroscopy on e.g. lung epithelial cells [19], quantum dots in aqueous solutions [19], and mRNAs in brain tissue [20]. Vermaas et al. [21] successfully employed MCR on hyperspectral confocal fluorescence images to obtain new structural information regarding the distribution and relative concentration of photosynthetic pigments in cyanobacteria. Actually, they in vivo localised photosynthesis related pigments (chlorophylls, phycobilins, and carotenoids) in wild-type and mutant cells of the cyanobacterium Synechocystis sp. PCC 6803. In the microarray technology field, Haaland et al. [22] demonstrated the applicability of MCR using data from a hyperspectral fluorescence imaging microarray scanner for monitoring gene expression in cells from thousands of genes on the array. Another modelling approach consists on establishing a multivariate regression that can be used to predict the concentrations of interest in every single pixel in the image. Such a model can be obtained on homogeneous samples with known chemical composition, and then be applied on images of heterogeneous samples. This approach has been reported to work well for on-line NIR systems estimating fat content in meat trimmings [23] and food content in crabs [24].

The objective of this article is to demonstrate how multispectral imaging based on front face fluorescence can be used for detailed studies of oxidation and photooxidation processes in cod caviar paste. In particular it is shown that it is possible to make images of the spatial distribution of sensory properties related to oxidation, which to our knowledge has not been done before. Cod caviar paste was used as a case product and it was stored over time to obtain a relevant span in lipid oxidation and sensory properties. A sensory panel was used to assess the sensory properties of a calibration and a test set based on homogeneous samples. Spectral images of these homogeneous samples were obtained and multivariate models based on both MCR and partial least squares regression (PLSR) were constructed and tested. These models were then applied on images of heterogeneous samples with gradients in oxidation and chemical properties.

2. Materials and methods

2.1. Materials

Twenty Kg of cod caviar paste were provided as a homogeneous batch from Mills (Mills DA, Oslo, Norway). It was packaged under vacuum and stored in the dark at 4 °C.

For the experiment, 250 g aliquots of caviar paste were placed in $195 \times 132 \times 25$ mm^3 thermoformed trays (Jihå Plast AB, Karlskoga, Sweden) made of A-PET/PE sheet (Wipak Oy, Nastola, Finland). The trays were sealed with a laminate film based on oriented polyester, Biaxer 65 XX HFP AF (Wipak Oy, Nastola, Finland; O_2 transmission rate of 5 cm^3/24 h at 23 °C, 50% relative humidity) with a 511VG tray-sealing machine (Polimoon, Kristiansand, Norway). The gas in all the packages was N_2 with traces of O_2 (0.03 ± 0.03%). Once the samples were packed, small holes were opened in the film, to let air in, for the samples to be stored in the presence of 21% O_2. For the preparation of samples to be stored with 1% O_2 in the headspace, air was injected through a septum with a syringe upto the target O_2 concentration. Measurements of the concentration of O_2 in the headspace were made with an O_2/CO_2 analyser (CheckMate 9900 O2/CO2, PBI-Dansensor A/S, Denmark). All trays were wrapped in one layer of transparent plastic film (Clingfilm, Toro, Norway) to avoid the loss of humidity.

2.2. Experimental design

An experimental design including storage time, light exposure, and O_2 headspace-concentration was created in order to obtain a large but relevant span in quality properties of cod caviar paste. Three different atmospheres were employed for the storage of the samples (anaerobic conditions with 100% N_2, 1% O_2, and 21% O_2). Some samples were exposed to light, while others were stored in the dark. The storage design and conditions for the calibration and test sets of samples are summarised in Table 1. A code was assigned to each sample, indicating the days of storage, the presence (L) or absence (D) of light exposure during storage, and the concentration of O_2 in the headspace (Table 1). The codes employed in this table will be further used to identify the samples

Table 1
Assayed storage conditions and sample coding for the calibration and test sets.

Storage time (days)	Calibration set					Test set			
	Light			Dark		Light			Dark
	0% O_2 (100% N_2)	1% O_2	21% O_2	0% O_2 (100% N_2)	21% O_2	0% O_2 (100% N_2)	1% O_2	21% O_2	
1	1L0		1L21	1D0	1D21				
4	4L0	4L1	4L21		4D21			T-4L21	
8						T-8L0	T-8L1	T-8L21	
10							T-10L1	T-10L21	
12	12L0	12L1	12L21		12D21				
15								T-15L21	
21	21L0		21L21	21D0	21D21				

throughout the article. The two trays containing 250 g of cod caviar paste and a third one containing two sample cuvettes filled up with cod caviar paste were stored under each condition detailed in Table 1. The caviar paste in the trays was used for sensory evaluation and TBARS, while caviar paste in the cuvettes was used for multispectral imaging of autofluorescence. Thus, the calibration and test sets were made up by 32 and 14 trays of caviar paste and 32 and 14 cuvettes, respectively. The test set was generated and measured 6 weeks after the calibration set, with the objective of validating the performance of the model.

A third set of samples were prepared directly in cuvettes. The sample surface of these was covered with rounded pieces (55-mm diameter) of 1-mm thick black cardboard with different patterns cut in them for light transmission. The different patterns simulated possible holes or faults in the caviar paste container. This would ensure light exposure of some parts of the samples and not of others. The cuvettes were placed inside metallic rings whose profile was slightly higher than those of the cuvettes, and the cardboard pieces were fixed on those rings with adhesive tape, to avoid contact with the sample surface. The whole set was wrapped in one layer of transparent film (Clingfilm, Toro, Norway) to avoid loss of humidity. The same patterns were assayed for short and long term exposures of 20 h and 14 days, respectively. A total of six different patterns were assayed, both under short and long term exposure conditions.

The light exposure was performed in a cold-storage chamber at 4 °C with fluorescent light tubes (Osram L 58W/954 Lumilux de Luxe-Daylight) placed vertically at a distance of approximately 9 cm from the trays. Trays were randomly moved during the exposure period, in order to assess an equal illumination for all of them.

2.3. Sensory analysis

Sensory analysis is a scientific discipline that applies principles of experimental design and statistical analysis to the use of human senses (sight, smell, taste, touch, and hearing) for the purposes of evaluating consumer products. The discipline requires panels of human assessors, on whom the products are tested, and recording the responses made by them.

The sensory evaluation was performed by a trained sensory panel at Nofima AS using descriptive sensory profiling according to Lawless and Heymann [25] and ISO standards [26]. The sensory panel consisted of ten selected and independent assessors [27] and took place in a purpose built sensory laboratory [28]. Prior to the analysis, the panel was trained in the definition and intensities of the chosen attributes, using caviar paste with varying sensory properties (samples 1D0 and 21L21 for the calibration set and a fresh sample, non-exposed and packed under vacuum, and T-15L21 for the test set). The assessed sensory attributes (in the same order as they were evaluated by the assessors) were: fresh and rancid odours and fresh, bitter, metallic, fish oil and rancid flavours. Those attributes have been previously described by us and successfully applied to characterise cod caviar paste from the sensory point of view [11].

Before evaluation, the samples in the trays were homogenised by stirring with a spoon. Then each assessor was served a teaspoon of caviar paste sample each on a cardboard plate at room temperature. Each sample was served twice and the serving order was randomized according to sample and assessor. Water and cucumber dices were provided to cleanse the palate between samples. A continuous non-structured scale was used for evaluation of sensory attributes. Each judge evaluated the samples at individual speed on a computer system for direct recording of data (Compusense five, v. 4.6; Compusense, Inc., Guelph, ON, Canada), and their scores were transformed to numbers from 1 (=no intensity) to 9 (=high intensity). The sensory score for each sample of caviar paste was obtained by averaging the individual scores from the 10 assessors for each of the 10 subsamples. A total of 64 samples were evaluated in the calibration set, and the measurements had to be carried out over 2 days due to capacity limitation; 28 samples were evaluated in the test set, 6 weeks later.

2.4. Thiobarbituric acid reactive substances (TBARS)

The 2-thiobarbituric acid reactive substances (TBARS) assay was performed by a method slightly modified from the previously proposed by Buege and Aust in 1978 [29]. Duplicate samples of caviar paste (0.10 g) were mixed with 3.0 mL aliquots of a stock solution containing 0.375% of 2-thiobarbituric acid (TBA) (Sigma Chemical Co., St. Louis, MO), 15% trichloroacetic acid (TCA) (Merck KGaA,Germany), and 0.25 N HCl. The mixture was vortexed and then heated for 10 min in a boiling water bath (100 °C) until development of a brownish colour. Later, it was cooled under tap water and centrifuged at 5500 rpm for 25 min. A 0.50 mL aliquot of the supernatant was transferred into the measurement cell and further diluted with 2.50 mL of ultrapure water. The absorbance of the resulting solution was measured at 532 nm (Ultraspec 3000, Pharmacia Biotech, Cambridge, U.K.), against a blank which contained all the reagents, except the caviar paste, treated exactly in the same way as described above. The absorbance measurements were normalised dividing them by the exact weight of cod caviar paste taken in each case. The normalised $A_{532\ nm}$ values, further referred to as the TBARS index, were employed to look for correlations with fluorescence data.

2.5. Multispectral imaging of autofluorescence

Samples were placed into sample cuvettes, which exposed a flat circular surface (19.6 cm^2) with a diameter of 5 cm for the measurements. Images were acquired with an optical bench

system previously described in detail by Wold et al. [30] and Wold and Kvaal [31] in a laboratory with a minimum of stray light. The excitation light was generated by a 300 W xenon arc lamp and a 10 nm bandwidth interference filter. The light was directed onto samples at an angle of about 45° and the lamp distance was adjusted to obtain a homogeneous illumination of the whole sample surface as possible. The camera was CCD cooled to −40 °C. An imaging spectrograph and a Nikon 102 mm photographic lens were connected to the CCD. Exposure time was 10 s for each image channel. Spectrograph, detector and camera were controlled by the software WinSpec 1.4.3.4.

In a previous work on fluorescence spectroscopy and cod caviar paste [11] we showed that the excitation wavelength of 382 nm is suitable to detect the generation of oxidation products which fluoresce in a broad band around 470 nm, as well as to monitor the bleaching of protoporphyrin IX (PpIX) (em=635 nm and 705 nm) and the formation and further bleaching of its main photoproduct photoprotoporphyrin (PPp) (em=670 nm). Thus, the excitation wavelength for this multispectral imaging experiment was common for all the channels and set to 382 nm (Table 2). The selection of emission-filters, detailed in Table 2, was based on our previous knowledge about the fluorescent behaviour of cod caviar paste system [11]. The autofluorescence emission spectra registered for a fresh cod caviar paste sample (1D0) and samples packaged in air and exposed to light for 1 (1L21) and 21 days (21L21) are shown in Fig. 1. In the spectrum of the fresh sample, two sharp peaks corresponding to PpIX at 635 and 705 nm are observed. After one day of exposure to light (sample 1L21) a decrease in the intensity of these peaks is observed and the appearance of a new peak centred at 670 nm, corresponding to PPp. [11] The spectra of both samples, 1D0 and 1L21, are quite similar for wavelengths below 600 nm. On the other hand, the emission spectrum of a sample exposed to light for 21 days (21L21) is characterised by the total bleaching of PpIX and PPp, and a broad emission band peaking around 470 nm is observed. This broad band arises from different stable fluorescent oxidation products [11]. Those three spectra represent the span of fluorescent properties of cod caviar paste under the given experimental design. Vertical lines in Fig. 1 represent the central wavelength of the selected emission-filters and the shaded areas around them represent their bandwidth (10 or 40 nm). A total of 11 filters along the whole wavelength region of interest were selected and strategically placed at wavelengths where important changes in the emission profiles take place, in order to collect as much chemical information as possible. Thus, autofluorescence images for a total of 32 and 14 cuvettes integrating calibration and test sets, respectively, and 12 cuvettes corresponding to the six assayed patterns submitted to short and long term light exposure, were obtained at every single emission wavelength.

Table 2
Filters and settings used for image acquisition

Channel	Excitation wavelength (nm)	Emission wavelength (nm)	Bandwidth (nm)
1	382	450	40
2	382	460	10
3	382	480	10
4	382	500	40
5	382	510	10
6	382	530	10
7	382	550	40
8	382	600	40
9	382	640	10
10	382	670	10
11	382	700	40

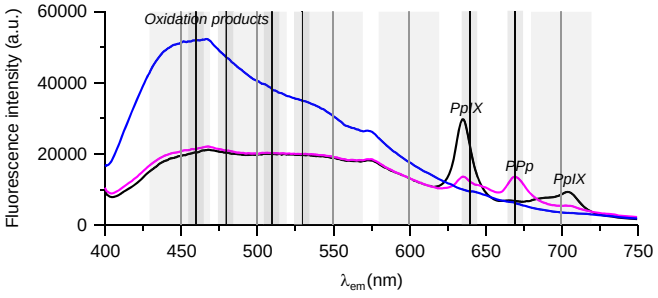

Fig. 1. Fluorescence emission spectra (λ_{ex}=382 nm) corresponding to a fresh cod caviar paste sample (1D0: ——) and two samples packaged in air and exposed to light for 1 (1L21: ——) and 21 days (21L21: ——). The emission band corresponding to oxidation products and the peaks for protoporphyrin IX (PpIX) and photoprotoporphyrin (PPp) have been labelled. Vertical lines are placed at the emission wavelengths of the assayed channels and the shaded areas around them represent the bandwidth of the filters (10 (——) or 40 nm (——)).

2.6. Image pre-Processing

Images of calibration and test samples were median-filtered through a 3-by-3 window to remove possible spikes and black points from "dead" pixels in the CCD. The illumination of the samples surface was not homogeneous over the whole surface and a slight illumination gradient was detected. A reference sample of white paper was imaged in the 11th image channel (ex=382 nm; em=700 nm), under the same conditions, to be used to compensate for this inhomogeneity. The reference image was also median-filtered and normalised to a maximum pixel value of 1. Each channel in the multispectral image was corrected by dividing it pixel by pixel by the reference image. The same reference image was used to correct all the channels of the multispectral images, the calibration and test sets as well as the images of the heterogeneous samples. Central rectangular areas of 130 pixels × 156 pixels (3.4 cm × 4.1 cm, 14.2 cm^2) were selected from calibration and test images, and further resized to 10 pixels × 10 pixels by binning for reasons of simplicity and to speed up the

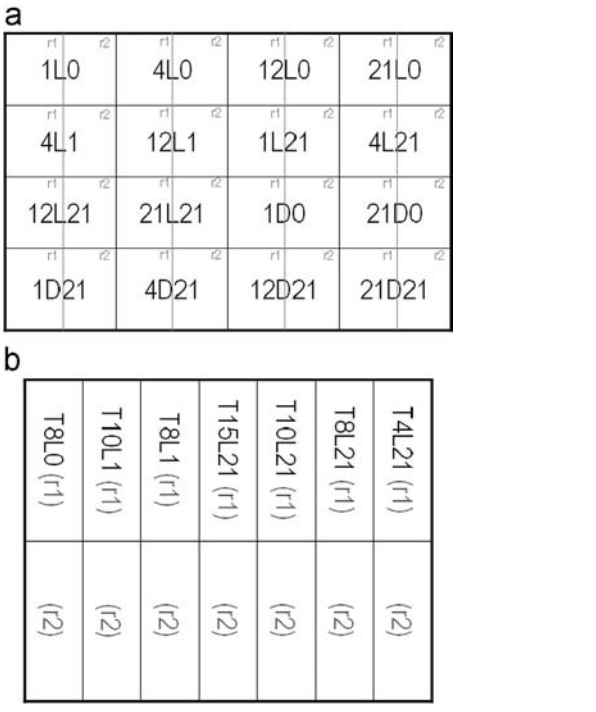

Fig. 2. Distribution of samples in each slice of the calibration (a) and test (b) 3D-arranges. r1 and r2 refers to replicates 1 and 2 of each sample.

calculations. The rectangular sub-sections extracted from the samples of the calibration and test sets were joined in two multispectral images, respectively, and organised as detailed in Fig. 2. Thus, the dimensions of images for the calibration and test sets were 40 pixels × 80 pixels × 11 wavelength channels and 20 pixels × 70 pixels × 11 wavelength channels, respectively.

Images of heterogeneous samples were median-filtered and corrected with the reference image as detailed above; then the central rectangular area of 130 pixels × 156 pixels was extracted. The dimension of the multispectral images obtained for each of these samples was 130 pixels × 156 pixels × 11 wavelength channels.

2.7. Data analysis

The analysis of images was carried out in two stages. First, MCR was used to estimate the main fluorescent components in the system to obtain chemical images of the caviar. Second, multivariate regression models were constructed for sensory attributes and TBARS, which could be used to create sensory images.

2.7.1. Multivariate curve resolution

MCR calculates spectral components that can be close to the pure fluorescent components and their corresponding relative concentrations in each sample. The algorithm and basis for MCR is described in detail by Tauler [32] and Tauler et al. [33]. Here, only a brief summary of the method is given. It is a usual assumption in MCR that the experimental data follows a linear model, which in matrix form can be written as

$$X = C\mathbf{S}^{\mathbf{T}} + \mathbf{E}$$

Where $\mathbf{X}$ is the data matrix with dimensions ($I \times J$), and $\mathbf{C}$ ($I \times N$) and $\mathbf{S}$ ($J \times N$) are matrices containing estimated concentration and spectra of pure chemical components, respectively. N is the number of pure chemical components. $\mathbf{E}$ ($I \times J$) is the matrix of residuals not explained by the chemical species in $\mathbf{C}$ and $\mathbf{S}$, and which hopefully is close to the experimental error. The main goal of curve resolution is the determination of the true $\mathbf{C}$ and $\mathbf{S}$ matrices based on the analysis of matrix $\mathbf{X}$.

Initial estimations of $\mathbf{C}$ or $\mathbf{S}$, which can be available from techniques based on the detection of the purest variables [34] or from techniques based on evolving factor analysis [35], are optimised solving the last equation iteratively by alternating least squares optimisation [36]. At each iteration of the optimisation, new estimation of the $\mathbf{C}$ and $\mathbf{S}$ matrices is obtained

$$\mathbf{C}^{+}\mathbf{X}^{*} = \mathbf{C}^{+}\mathbf{C}\mathbf{S}^{\mathbf{T}} = \mathbf{S}^{\mathbf{T}}$$

and

$$\mathbf{X}^{*}\left(\mathbf{S}^{\mathbf{T}}\right)^{+} = C\left(\mathbf{S}^{\mathbf{T}}\right)\left(\mathbf{S}^{\mathbf{T}}\right)^{+} = C$$

where the matrix $\mathbf{X}^{*}$ is the PCA reproduce data matrix for the selected number of components, the matrix $\mathbf{C}^{+}$ is the pseudoinverse of the matrix $\mathbf{C}$, i.e. $\mathbf{C}^{+} = \mathbf{C}(\mathbf{C}^{\mathrm{T}}\mathbf{C})^{-1}$ and the matrix $(\mathbf{S}^{\mathrm{T}})^{+}$ is the pseudoinverse of the matrix $\mathbf{S}^{\mathrm{T}}$. At each iterative cycle, the non-negativity constraint was applied. The constrained iterative optimisation was carried out until convergence was achieved.

MCR has been successfully extended to the study of second order three-way data matrices [32,37,38]. The commonly followed strategy implies the analysis of unfolded column-wise data matrices. Thus, in order to implement MCR on our three dimensional array of data, the calibration image was unfolded from dimensions 40 × 80 × 11 to 3200 × 11, and on this two-dimensional array, MCR was applied. The array of MCR estimated concentrations was then refolded to its original image format, resulting in potential chemical images.

In the present work, first of all, the calibration dataset was analysed

$$\mathbf{X}_{cal} = \mathbf{C}_{cal}\mathbf{S}_{cal}{}^{T} + \mathbf{E}$$

and $\mathbf{C}_{\mathrm{cal}}$ and $\mathbf{S}_{\mathrm{cal}}$ were calculated. Then, the obtained spectral profiles $\mathbf{S}_{\mathrm{cal}}$, were employed to estimate the concentration of pure chemical components in the unfolded test set image and on the unfolded images of heterogeneous samples

$$\mathbf{C}_{\mathrm{test}} = \mathbf{X}_{\mathrm{test}}\mathbf{S}_{\mathrm{cal}}\left(\mathbf{S}_{\mathrm{cal}}{}^{\mathrm{T}}\mathbf{S}_{\mathrm{cal}}\right)^{-1}$$

or

$$\mathbf{C}_{\mathrm{het}} = \mathbf{X}_{\mathrm{het}}\mathbf{S}_{\mathrm{cal}}\left(\mathbf{S}_{\mathrm{cal}}{}^{\mathrm{T}}\mathbf{S}_{\mathrm{cal}}\right)^{-1},$$

respectively.

MCR was performed in Matlab ver. 7.6.0 (R2008a) (The Mathworks Inc., Natick, MA) by use of the PLS_Toolbox (Eigenvector Research Inc., Wenatchee, WA).

2.7.2. Multivariate regression

Multivariate regression models were constructed based on the calibration image dataset (X) and the sensory assessed attributes and TBARS (Y). The constructed models were validated on the test set and further applied to predict pixel by pixel the sensory attributes and TBARS on heterogeneous samples, which allowed us to obtain sensory images.

Partial least-squares regression (PLSR) [39] was employed to construct the calibration models between fluorescence data and sensory and TBARS values. The optimal number of PLSR factors of the calibration models was determined by segmented cross-validation, leaving out the pixel spectra from two replicates corresponding to the same storage conditions at the same time. The validation method provided a predicted value $\hat{y}_i (i=(1,\ldots,i,\ldots N))$ which was compared with the reference value, y_i (sensory or TBARS). The multivariate prediction correlation coefficient (R) and the prediction error, expressed as root mean square error of cross-validation (RMSECV), were used as quality criteria to evaluate the models. RMSECV is defined as

$$\mathrm{RMSECV} = \sqrt{\frac{1}{N}\sum_{i=1}^{N}(y_i - \hat{y}_i)^2},$$

where i denotes the samples from 1 to N. RMSECV represents the average uncertainty that can be expected when predicting Y-values for new samples.

The constructed calibration models were used for the prediction of reference values of sensory attributes and TBARS for the test set samples. Model performance was reported as the root mean square error of prediction (RMSEP), calculated exactly as RMSECV (being $\hat{y}_i$ a result of prediction and not cross-validation), and the multivariate correlation coefficient (R). PLSR was performed with the software The Unscrambler (v. 9.8, Camo AS, Oslo, Norway).

The employed fluorescence spectra for the construction of these models were the average spectra of each sample in the calibration set. In the case of the regression for sensory attributes, PLS2 regression was employed. PLS2 is a version of PLSR which allows simultaneous modelling of several Y-variables (sensory attributes in this case) taking advantage of possible correlations or co-linearity between them [39]. PLS1 was used for the TBARS model. For validation, the regression vectors were applied on the average fluorescence spectrum of each of the test samples. The regression vectors were then employed pixel-wise on heterogeneous images to obtain sensory images.

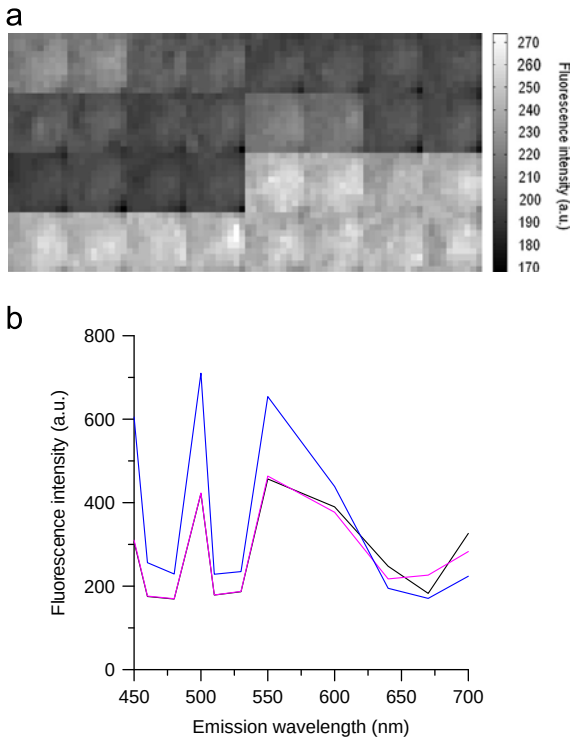

Fig. 3. (a) Registered images for calibration samples in channel 9 (λ_{ex}=382 nm and λ_{em}=640 nm). (b) Mean spectra extracted from images of replicate one (r1) of samples 1D0 (——), 1L21 (——), and 21L21 (——).

3. Results and discussion

Band number nine (ex=382 nm; em=640 nm) of the multispectral image of the calibration set is shown in Fig. 3(a). Each squared area corresponds to one sample of the calibration set, according to the sample organisation shown in Fig. 2. The colour-bar represents the fluorescence intensity: the brighter a given area is, the stronger the fluorescence is. Channel nine is close to the emission peak of PpIX at 635 nm and that is why the samples kept in the dark have high intensities in this channel. The mean spectra obtained from images for replicate 1 of samples 1D0, 1L21 and 21L21 are also shown in Fig. 3(b). These are the same samples as shown with high-resolution emission spectra in Fig. 1. The spectral resolution in the image data is much lower and the spectral shapes are not as clear as for the high-resolution ones, shown in Fig. 1. The main distortion of the shape is due to the different transmission properties of the emission filters at the different channels. However, the same main spectral features can be found: higher intensities at 640 and 700 nm for the fresh sample, due to the higher concentration of PpIX; decrease of the intensity at these two emission wavelengths and increase of the intensity at 670 nm after one day of light exposure (sample 1L21), as a consequence of the photo-conversion of PpIX to PPp. The intensities at emission wavelengths below 600 nm were similar for samples 1D0 and 1L21; while the strongest emission of fluorescence between 450 and 600 nm was obtained for sample 21L21, arising from stable fluorescent oxidation products. The spectra for these samples express well the span in fluorescence properties in the current design and will help in further interpretation of the emission profiles for pure components calculated by MCR. It is possible to correct the image spectra for the differences in filter transmission properties, however, it would not have any other interest beyond the purely aesthetic.

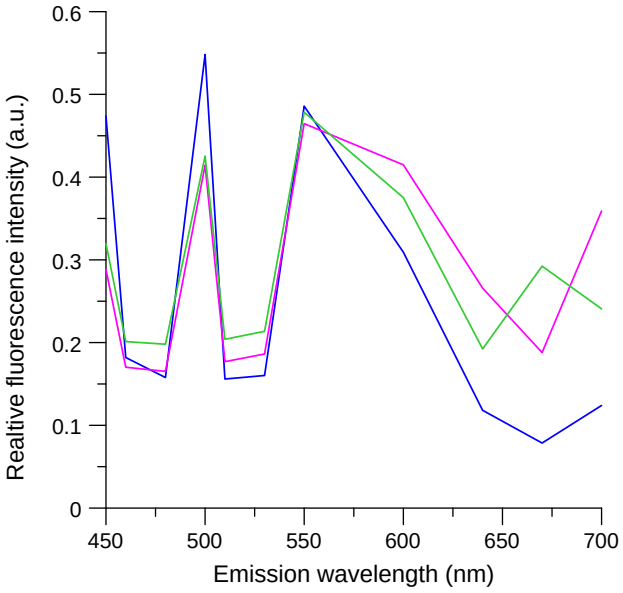

Fig. 4. Spectral emission profiles of the MCR-estimated pure components: component number 1 (——), component number 2 (——), and component number 3 (——).

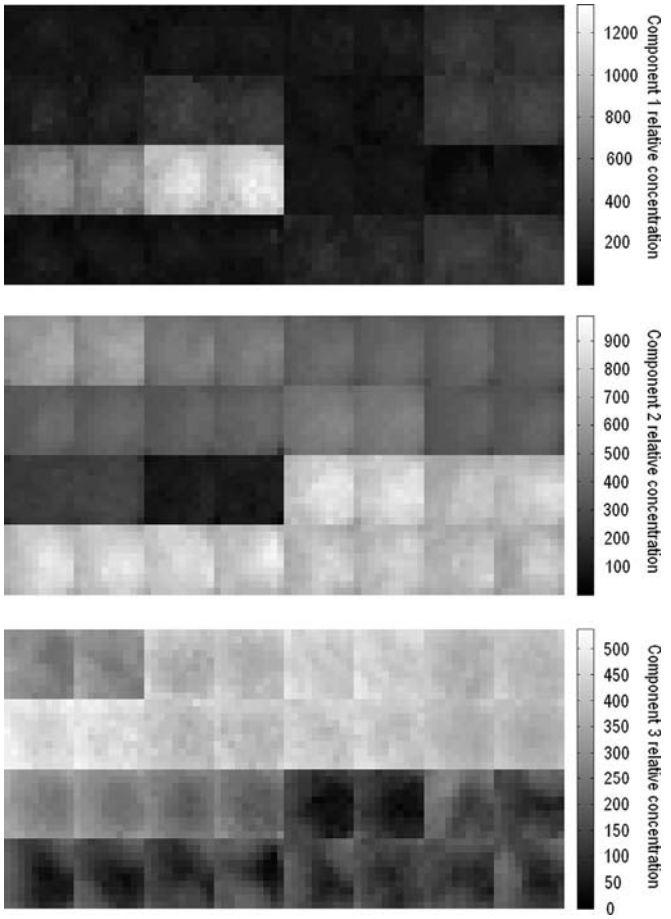

Fig. 5. MCR-estimated relative concentrations for the fluorescent components 1, 2 and 3.

3.1. Multivariate curve resolution—chemical images

The multispectral calibration set was decomposed by MCR. Three components were found to explain 98.7% of the spectral

data. The obtained emission profiles for the components are shown in Fig. 4. The shapes of the profiles are not very obvious, nevertheless it is possible to make an assignment and compare the estimated concentrations with expected concentrations in the samples. PpIX, PPp and oxidation products were the expected fluorescence components, [11] and as a result of the experimental design the intensity of these components should vary quite differently along sample sets.

Component one is characterised by low intensity at wavelengths longer than 600 nm and high intensities at 450, 500 and 550 nm. This suggests that it represents stable fluorescent oxidation products. Component number two has the highest intensity at 600, 640 and 700 nm, so it likely to represent PpIX, which has known emission peaks at 635 and 705 nm. Component number three is quite similar to component two in the 400–600 nm region, while it has a clear peak at 670 nm, which agrees with the spectral profile of PPp. It is obvious from Fig. 4 that the aim in this study is not to obtain very recognisable spectral components. The goal is that they actually represent the chemical compounds and can be used to estimate their concentrations. The assumed identification of the components and estimated concentrations should agree with the expected concentrations in the calibration set.

In Fig. 5 the calculated relative concentrations for each component are plotted for the calibration set (sample organisation shown in Fig. 2). Sample 21L21 had the highest relative concentration for component one, followed by sample 12L21. Samples stored in the dark and packed in anaerobium atmosphere (1D0 and 21D0) were characterised by the lowest concentration for this component (darkest areas in the image). These observations support the assignment of this component to fluorescent stable oxidation products. The concentration of component one along lowest sample row packed with air and stored in the dark increases slightly with time (from left to right) due to autoxidation. The concentration distribution for component 2 agrees with what we could expect for PpIX. An apparent total bleaching of PpIX was achieved after 21 days of exposure to light in the presence of air (sample 21L21). The sample with the highest concentration of PpIX was the fresher one: 1D0. Samples packed in air and kept in the dark showed a slight progressive decrease of the concentration of PpIX over time, suggesting that PpIX was involved as an antioxidant in autoxidation processes. Antioxidant effect of PpIX is also observed in anaerobium atmosphere: the same decrease in PpIX is observed in the presence or absence of oxygen in headspace: 21D0 and 21D21. Upper row shows samples packed in anaerobium conditions and exposed to light from 1 to 21 days (left to right). A progressive bleaching of PpIX was observed under these conditions. The third component was assumed to represent PPp, the photoproduct of PpIX. The estimated concentrations for this component support this assignment: photoreactions do not take place in the dark and explain why this component was absent for samples kept in the dark. For the samples packed in the absence of oxygen and exposed to light between 1 and 12 days, the concentration of PPp increased with time, while the concentration of PpIX decreased. PPp is known to be a photosensitizer itself, and after 21 days of storage under light exposure, a slight decrease was observed in its concentration. Also, connecting this image to the concentrations predicted for component 1, higher concentrations of oxidation products were found for this sample along the first row.

Based on spectral profiles and studies of concentrations, we conclude that the three MCR components are good representations of oxidation products, PpIX and PPp. The obtained spectral profiles were used to estimate relative concentrations of the three components in the heterogeneous images. These "chemical images" are shown in Fig. 6. As stated above, component 1 represents stable fluorescent oxidation products. These products are mainly Schiff base structures resulting from the interaction of unsaturated aldehydes with proteins or aminoacids [40–42]. The

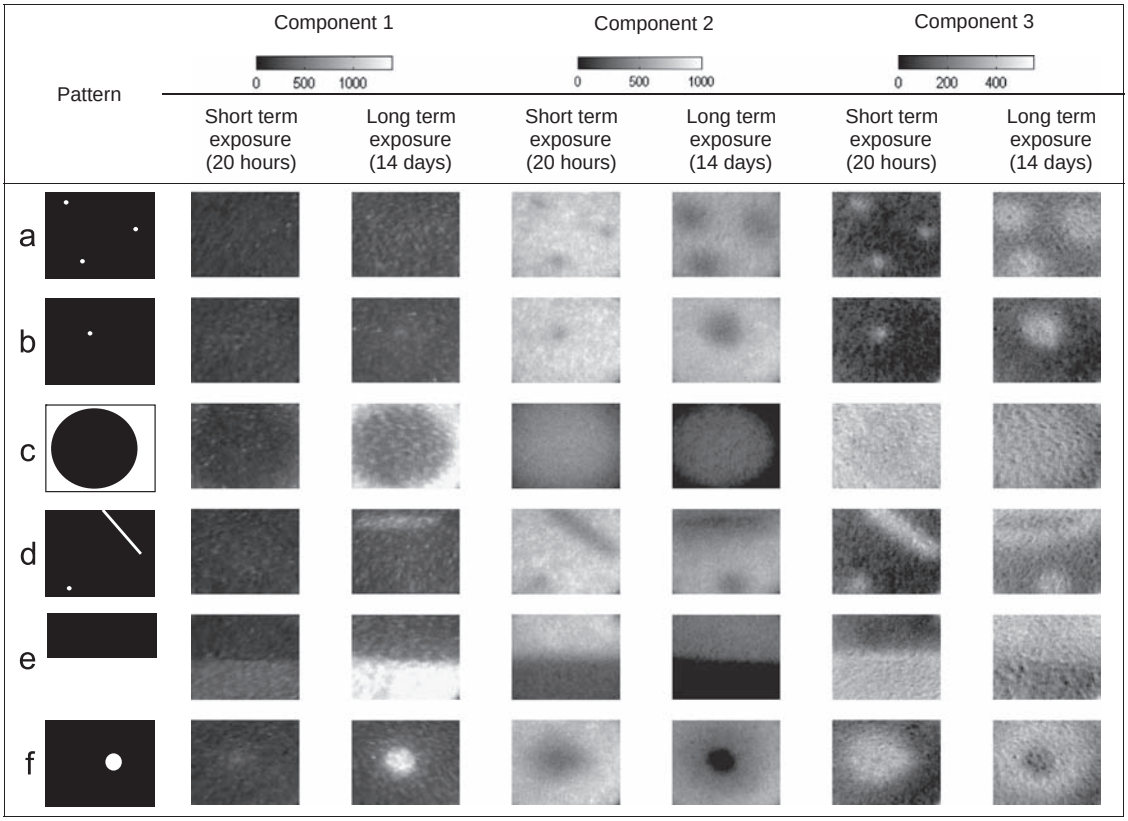

Fig. 6. Predicted concentrations for MCR-components 1, 2 and 3 in heterogeneous samples, according to the MCR-model constructed based on the calibration set.

Table 3
Results from partial least squares regression (PLSR) for some sensory-assessed attributes of interest (PLS2; #Factors=2) and TBARS (PLS1; #Factors=1) vs fluorescence (mean spectra).

Sensory attributes		Calibration ($N=32$)			Prediction ($N=14$)		
		R	RMSECV	Y_{cal} range	R	RMSEP	Y_{test} range
Odours	Fresh odour	0.35	1.0	2.5–5.5	0.91	0.57	3.2–5.3
	Rancid odour	0.62	0.74	1.0–3.7	0.86	0.47	1.1–3.0
Flavours	Fresh flavour	0.56	1.1	1.8–5.6	0.89	0.75	2.8–5.6
	Bitter flavour	0.78	0.32	4.6–6.1	0.75	0.31	4.6–5.6
	Metallic flavour	0.69	0.35	4.1–5.3	0.75	0.26	4.2–5.2
	Fish oil flavour	0.66	0.66	2.6–4.9	0.82	0.35	3.4–4.7
	Rancid flavour	0.69	1.1	1.1–5.2	0.88	0.58	1.4–4.7
TBARS-index		0.90	0.035	0.68–1.0	0.91	0.058	0.75–0.88

R gives the correlation coefficient; RMSCV is the root mean square error of cross-validation; RMSEP is the root mean square error of prediction.

formation of these products, as it is reported for several systems in general and cod caviar paste in particular [11] is not immediate and it takes some time until the concentration of such products is detectable. On the other hand, the photobleaching process of PpIX, and the successive formation of PPp are chemical processes taking place immediately at light exposure. This can be observed in the variation of the concentrations of components 1, 2 and 3 after 20 h of light exposure. Little or no increase was registered in the concentration of component one as a consequence of light exposure during 20 h. More clear is the decreased concentration of component two and increased concentration of component 3 in the exposed areas, representing PpIX photobleaching and PPp formation, respectively. In the set of samples exposed to light for 14 days, the concentration of component one, oxidation products, has increased, in particular in the light exposed areas. In the cases "a" and "b" (Fig. 6) it can be seen that a slight overall increase in oxidation had occurred, but not located to the small areas of light exposure. The increase might be a combination of auto-oxidation and photo-oxidation. Regarding component 2, a strong photobleaching of PpIX can be observed in the exposed zones. In the cases "a", "b" and "d" the photobleached areas were larger than the wholes of light exposure, and this can be ascribed to light scattering in the product. Lastly, the concentration of component three is high where samples were exposed through small holes, since the intensity of radiation reaching the sample surface was sufficient to transform PpIX to PPp. For larger exposed areas, where the light had been more intense, it could be observed that the photobleaching of the formed PPp had started to dominate. Case "f" (Fig. 6) represents an interesting example with a bright "donut". PPp was first generated over a large area due to light scattering. When there is little PpIX left, the photobleaching of PPp will dominate, and this will be most pronounced in the centre where light intensity is highest. Therefore, there is a dark central area where PPp was degraded. The same effect can be observed in case "d" along the exposed line, where the concentration of PPp was higher around the exposed line than in the actual line.

The results show that multispectral imaging of autofluorescence can be used to image important chemical constituents related to auto-oxidation and photo-oxidation in a complex matrix like cod caviar paste. The images can be used to follow they formation and degradation of these compounds and thereby the give the opportunity to monitor such oxidation processes in time and space. Similar fluorescent photosensitizers and stable fluorescent oxidation products as found in cod caviar paste has been reported for other systems [9,10], thus the proposed methodology could be used in those as well.

With MCR there will always be a challenge to obtain the correct true spectral components. For front-face fluorescence data it has been pointed out that reabsorption of fluorescence for e.g. pigments will affect the calculated profiles and also obscure the concentration estimates [43]. In the case of caviar, it has a pink-orange colour which is slightly bleached after light exposure. This bleaching could give a reduction of absorption in the blue region (400–500 nm) and slightly affect the intensity and shape of component 1. Components 2 and 3 would probably be unaffected by reabsorption.

3.2. Regression analysis – sensory Images

Regression results are summarised in Table 3. Two factors were selected as optimum for the PLS2 model for sensory attributes, which explained 99.87% and 96.01% of the total variance in X and Y-blocks, respectively. Fairly good multivariate correlation coefficients (R) were obtained when calibration models were cross-validated, probably due to the reduced number of samples and the low resolution in the employed calibration spectra. RMSECV ranged between 0.32 and 1.1. Nevertheless, high R values, ranging between 0.75 for bitter and metallic flavours and 0.91 for fresh odour, were obtained when the obtained models were validated by predicting sensory attributes of the test set. In the case of TBARS, one component was enough to explain 98.84 and 99.79% of the total variance in X and Y-blocks, respectively, and an R value of 0.9 was obtained both when the model was cross-validated and validated on the test set. The regression models corroborate that the low resolution image spectra successfully captured the spectral information needed to model TBARS and the assessed sensory attributes related to rancidity.

Care has to be taken when making conclusions based on regression vectors in multivariate regression [44]. In this case a logical interpretation related to the freshness and rancidity can be done. Regression vectors for fresh odour and flavour were characterised by high intensities for wavelengths longer than 600 nm and low intensities for wavelengths shorter than 600 nm (not shown). This matches the spectral features of a fresh sample. The shape of the regression vectors for rancid odour and flavour were more or less opposite, high values in the region 450–550 nm and very low values over 600 nm.

When applying the regression vectors to the images of heterogeneous samples, sensory images were obtained (Fig. 7). They show the distribution of fresh and rancid flavour after 20 h and 14 days in the same samples as shown in Fig. 6. Gradients in sensory properties can be observed corresponding to the pattern of light exposure. Within samples subjected to short term light exposure, loss of freshness and an increase in rancidity was observed only when the light exposed area was rather big, e.g. for case "e" or "f". For samples exposed through small holes or a narrow line (cases "a", "b" and "d"), no changes in sensory attributes were detected after 20 h of exposure to light. This relates well to the images of

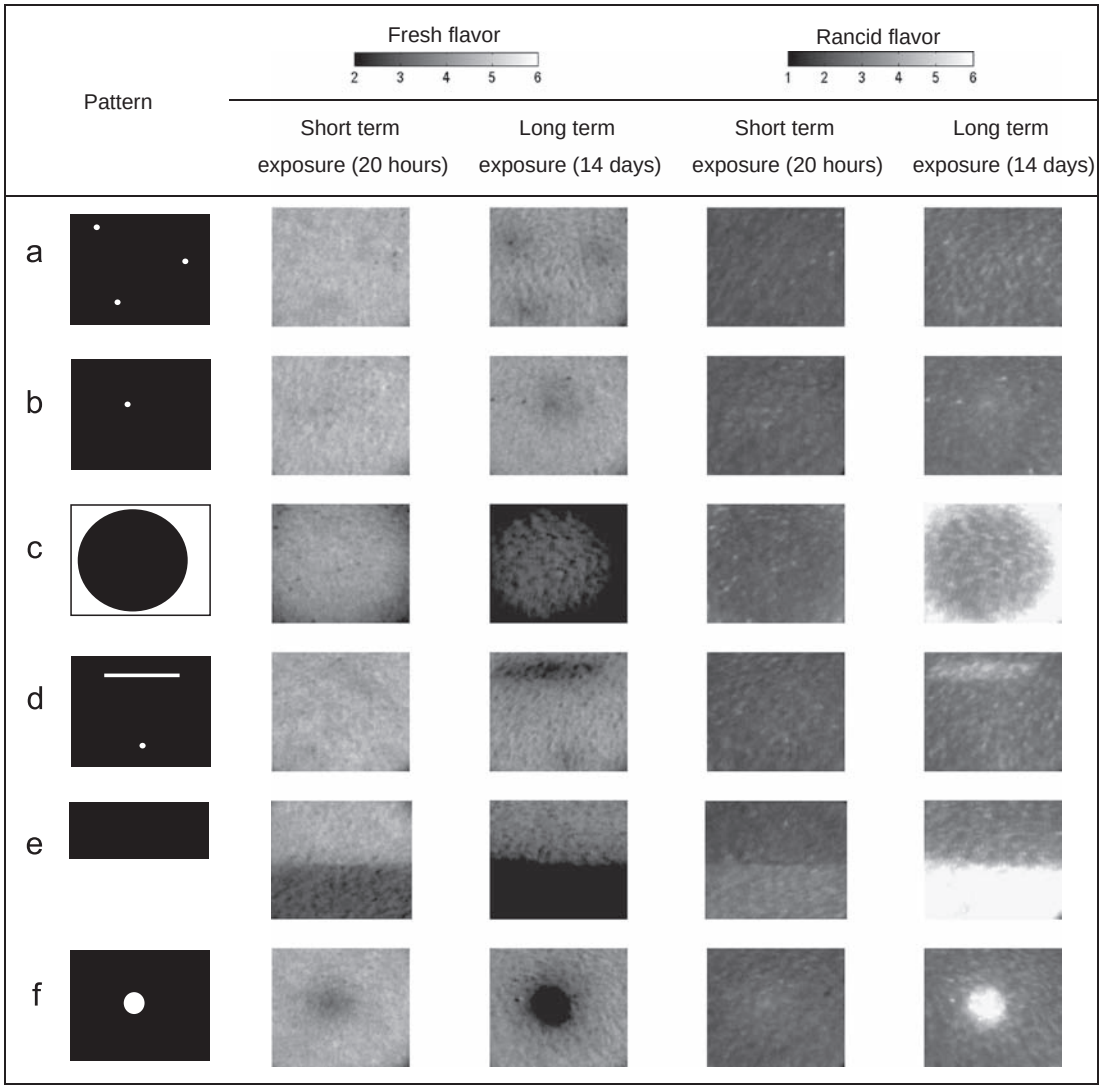

Fig. 7. Predicted fresh and rancid flavours for heterogeneous samples exposed to light for 20 h or 14 days.

MCR component 1 assigned to oxidation products (Fig. 6). These products were formed to only a limited extent after 20 h.

After 14 days of storage, the distribution of sensory properties reflects the patterns of light exposure quite well. A decrease in the fresh flavour and an increase in rancid flavour are obtained in all exposed areas, most easily seen when exposed areas were large. For case "a" and "b" it can be seen a slight overall decrease of fresh flavour, which can be ascribed to auto-oxidation. Some small darker regions corresponding to the pinholes can also be discerned. These darker regions can be ascribed to photo-oxidation. Images of TBARS were similar to those of rancid flavour and are therefore not shown.

In this study we used the average spectra from each sample in the calibration models. An alternative could be to include all single pixel spectra in the model. Then some of the natural image noise would have been included in the data, and more robust models might have been obtained. In this study we observed that the two approaches gave similar results. A discussion of such modelling approaches can be found in Wold and Kvaal [31].

The sensory images in Fig. 7 and the chemical images in Fig. 6 are of course very related. The chemical images show some of the chemical processes that result in the sensory images, but they do all carry different and specific information. It gives the interesting opportunity to compare the chemical information with the sensory information. The results also illustrates that curve resolution (MCR) and regression have two different purposes. Successful MCR enables imaging of specific chemical compounds, while regression in this case could be used to map more complex quality features into the image domain. The approach of making calibrations on homogeneous bulk samples, and then applying these calibrations pixel by pixel to study details in heterogeneous samples [23,24] is effective and can be recommended for quantitative multispectral imaging of other complex bio-systems. A well-defined calibration set is not needed for MCR. MCR can be applied directly on images of heterogeneous samples, however, a controlled sample set can be important in assisting the interpretation and validation of the model.

The imaging system used in this study was very slow (long exposure times) and of low spectral resolution. The main aim for us, however, was to illustrate the potential of chemical and sensory imaging based on spectral imaging of autofluorescence. Much more efficient, high resolution and more accurate systems are available, which enable faster and more detailed studies than the present. Such systems can be calibrated against sensitive, but slow and costly sensory panels, and then be used to capture detailed chemical and sensory images of oxidation progress in intact biomaterials.

4. Conclusions

It is demonstrated that multispectral imaging of autofluorescence in combination with multivariate curve resolution and partial least squares regression, is a well-suited methodology to map the concentration and distribution of fluorescent compounds and sensory assessed attributes in cod caviar paste. As far as we know this is the first time that sensory images of odours and flavours are obtained based on multispectral imaging. The methodology is a potent tool for investigation of the kinetics of auto-oxidation and photo-oxidation in complex intact biomaterials. The approach of making regression models based on homogeneous bulk samples, and then applying these calibrations pixel by pixel to study details in heterogeneous samples is effective and can be recommended for quantitative multispectral imaging of other complex bio-systems, also at the microscopic level.

References

[1] N. Intawiwat, A. Veberg Dahl, M.K. Pettersen, J. Skaret, E.O. Rukke, J.P. Wold, Int. Dairy J. 21 (2011) 531–539.
[2] G.M. Strasburg, R.D. Ludescher, Trends Food Sci. Technol. 6 (1995) 69–75.
[3] G.G. Guilbault, Practical Fluorescence, in: G.G. Guilbault (Ed.), Marcel Dekker, Inc., N.Y., 1990.
[4] C.A. Parker, Apparatus and experimental methods, in: C.A. Parker (Ed.), Photoluminescence of Solutions with Applications to Photochemistry and Analytical Chemistry, Elsevier, Amsterdam, The Netherlands, 1968, pp. 128–302.
[5] K.I. Hildrum, J.P. Wold, V.H. Segtnan, J.P. Renou, E. Dufour, in: L. Nollet, F. Toldra (Eds.), New spectroscopic techniques for online monitoring of meat quality; Advanced Technologies for Meat Processing, Taylor & Francis CRC Press, Boca Raton, Florida, 2006, pp. 87–123.
[6] A. Veberg, E. Olsen, G. Vogt, A.N. Nilsen, M. Mielnik, J.P. Wold, J. Food Sci. 71 (2006) 364–370.
[7] E. Olsen, A. Veberg, G. Vogt, O. Tomic, B. Kirkhus, D. Ekeberg, A. Nilsson, J. Food Sci. 71 (2006) 284–292.
[8] R. Karouia, E. Dufour, J. Baerdemaekera, Food Chem. 101 (2007) 1305–1314.
[9] J.P. Wold, A. Veberg Dahl, F. Lundby, A.N. Nilsen, A. Juzeniene, J. Moan, J. Photochem. Photobiol. 85 (2009) 669–676.
[10] J.P. Wold, A. Veberg, F. Lundby, A.N. Nilsen, J. Moan, Int. Dairy J. 16 (2006) 1218–1226.
[11] D. Airado-Rodriguez, J. Skaret, J.P. Wold, J. Agric. Food Chem. 58 (2010) 5276–5285.
[12] N. Lamei, K.D. Hutchison, M.M. Crawford, N. Khazenie, Opt. Eng. 33 (1994) 1303–1313.
[13] S. Anderson-Engels, J. Johansson, S. Svanberg, Appl. Opt. 33 (1994) 8022–8029.
[14] B. Vekemans, K. Janssens, L. Vincze, A. Aerts, F. Adams, J. Hertogen, X-ray Spectrom. 26 (1997) 333–346.
[15] M.R.F. Lee, V.J. Theobald, H.J. Ougham, A. Veberg Dahl, F. Lundby, N.D. Scollan, J.P. Wold, Meat Sci. 86 (2010) 966–975.
[16] S. Andersson-Engels, C. Klinteberg, K. Svanberg, S. Svanberg, Phys. Med. Biol. 42 (1997) 815–824.
[17] G.A. Wagnieres, W.M. Star, B.C. Wilson, Photochem. Photobiol. 68 (1998) 603–632.
[18] J.P. Wold, I.R. Johansen, K.H. Haugholt, J. Tschudi, J. Thielemann, V.H. Segtnan, B. Narum, E. Wold, J. Near Infrared Spectrosc. 14 (2006) 59–66.
[19] D.M. Haaland, H.D. Jones, M.H. Van Benthem, M.B. Sinclair, D.K. Melgaard, C.L. Stork, M.C. Pedroso, P. Liu, A.R. Brasier, N.L. Andrews, D.S. Lidke, Appl. Spectrosc. 63 (2009) 271–279.
[20] V.L. Sutherland, J.A. Timlin, L.T. Niemanb, J.F. Guzowski, M.K. Chawla, P.F. Worley, B. Roysame, B.L. McNaughton, M.B. Sinclair, C.A. Barnes, J. Neurosci. Methods 160 (2007) 144–148.
[21] W.F.J. Vermaas, J.A. Timlin, H.D.T. Jones, M.B. Sinclair, L.T. Nieman, S.W. Hamad, D.K. Melgaard, D.M. Haaland, Proc. Natl. Acad. Sci. USA 105 (10) (2008) 4050–4055 (Available)⟨http://www.pnas.org/content/105/10/4050.full.pdf+html⟩.
[22] Haaland D.M., Timlin J.A., Sinclair M.B., Van Benthem M.H., Martinez M.J., Aragon A.D., Werner-Washburne M., Multivariate curve resolution for hyperspectral image analysis: applications to microarray technology, in:Richard M. Levenson, Gregory H. Bearman, Anita Mahadevan-Jansen (Eds.), Proceedings of SPIE, Spectral Imaging: Instrumentation, Applications, and Analysis II, vol. 4959, SPIE, Bellingham, WA, 2003, pp. 55–66
[23] J.P. Wold, M. O'Farrel, M. Høy, J. Tschudi, Meat Sci. 89 (2011) 317–324.
[24] J.P. Wold, M. Kermit, A. Woll, Appl. Spectrosc. 64 (2010) 691–699.
[25] H.T. Lawless, H. Heymann, Sensory Evaluation of Food: Principles and Practices, Chapman & Hall, New York, 1998.
[26] ISO 13299, Sensory analysis-methodology-general guidance for establishing a sensory profile, International Organization for Standardization, Geneva, Switzerland, 2003.
[27] ISO 8586, Sensory analysis methodology-general guidance for the selection, training and monitoring of Assessors, part 1: Selected Assessors, 1st ed., International Organization for Standardization, Geneva, Switzerland, 1993.
[28] ISO 8589, Sensory analysis methodology-general guidance for the design of test rooms, International Organization for Standardization, Geneva, Switzerland, 1988.
[29] J.A. Buege, S.D. Aust, Methods Enzymol. 52 (1978) 302–310.
[30] J.P. Wold, K. Kvaal, B. Egelandsdal, Appl. Spectrosc. 53 (1999) 448–456.
[31] J.P. Wold, K. Kvaal, Appl. Spectrosc. 54 (2000) 900–909.
[32] R. Tauler, Chemom. Intell. Lab. Syst. 30 (1995) 133–146.
[33] R. Tauler, A. Smilde, B. Kowalski, J. Chemom. 9 (1995) 31–58.
[34] W. Windig, J. Guilment, Anal. Chem. 63 (1991) 1425–1432.
[35] R. Tauler, E. Casassas, J. Chemom. 3 (1989) 151–161.
[36] R. Tauler, E. Casassas, A. Izquierdo-Ridorsa, Anal. Chim. Acta 248 (1991) 447–458.
[37] R. Tauler, B.R. Kowalski, S. Flemming, Anal. Chem. 65 (1993) 2040–2047.
[38] R. Tauler, D. Barceló, Trends Anal. Chem. 12 (1993) 319–327.
[39] H. Martens, T. Naes, Multivariate Calibration, U.K., Wiley, Chichester, 1989.
[40] A. Veberg, G. Vogt, J.P. Wold, LWT-Food Sci. Technol. 39 (2006) 562–570.
[41] S. Yamaki, T. Kato, K. Kikugawa, Chem. Pharm. Bull. 40 (1992) 2138–2142.
[42] J.H. Liang, Food Chem. 66 (1999) 103–108.
[43] L. Lakhal, V. Acha, T. Aussenac, Chemom. Intell. Lab. Syst. 116 (2012) 112–122.
[44] C.D. Brown, R.L. Green, Trends Anal. Chem 28 (2009) 506–514.